Biogeosciences Discuss., 10, 3891–3923, 2013
www.biogeosciences-discuss.net/10/3891/2013/
doi:10.5194/bgd-10-3891-2013

Biogeosciences Discussions
Open Access

Inter-shelf nutrient transport from the East China Sea as a major nutrient source supporting winter primary production on the northeast South China Sea shelf

A. Han[1], M. Dai[1], J. Gan[2], S.-J. Kao[1], X. Zhao[2], S. Jan[3], Q. Li[1], H. Lin[1], C.-T. A. Chen[4], L. Wang[1], J. Hu[1], L. Wang[1], and F. Gong[5]

[1]State Key Laboratory of Marine Environmental Science, Xiamen University, Xiamen, China
[2]Division of Environment, Hong Kong University of Science and Technology, Kowloon, Hong Kong, China
[3]Institute of Oceanography, National Taiwan University, Taipei, China
[4]Institute of Marine Geology and Chemistry, National Sun Yat-Sen University, Kaohsiung, China
[5]State Key Laboratory of Satellite Ocean Environment Dynamics, Second Institute of Oceanography, State Oceanic Administration, Hangzhou, China

Received: 25 November 2012 – Accepted: 9 January 2013 – Published: 28 February 2013

Correspondence to: M. Dai (mdai@xmu.edu.cn)

Published by Copernicus Publications on behalf of the European Geosciences Union.

Abstract

The East China Sea (ECS) and the South China Sea (SCS) are two major marginal seas of the north Pacific with distinct seasonal primary productivity. Based upon field observation in December 2008–January 2009 covering both the ECS and the northern SCS (NSCS) in wintertime, we examined southward long-range nutrient-transport from the ECS to the northeast SCS (NESCS) carried by the China Coastal Current (CCC) driven by the northeast prevailing monsoon. These nutrients escaped from the cold ECS shelf to refuel the primary production on the NESCS shelf where river-sourced nutrients were limited yet water temperature remained favorable. By coupling the field observation of nitrate+nitrite (DIN) with the volume transport of the CCC, we derived a first order estimate of DIN flux of $\sim 1430 \pm 260\,\mathrm{mol\,s^{-1}}$. This DIN flux was ~ 7 times the wintertime DIN input from the Pearl River, a primary riverine nutrient source to the NSCS. By assuming DIN was the limiting nutrient, such southward DIN transport would have stimulated $\sim 8.8 \pm 1.6 \times 10^{11}$ gC of new production (NP), accounting for $\sim > 58 \pm 10$ % of the total NP or $\sim 38 \pm 7$–24 ± 4 % of primary production on the NESCS shelf shallower than 100 m.

1 Introduction

The continental shelf is well known to be characterized by high biological production, due to the abundant nutrient sourced from the land via river discharge and/or supplied through coastal upwelling and shoreward cross-shelf transport (Wollast, 1991, 1993; Ladd et al., 2005; Whitney et al., 2005; Sugimoto et al., 2009). Another possible transport pathway to redistribute dissolved and particulate nutrients and materials is through alongshore currents typically along the isotherms featured with long distance volume transport (Liu et al., 2000; Kao et al., 2003; Keafer et al., 2005; Whitney et al., 2005; Liu et al., 2007; Chen, 2008; Guo et al., 2012). However, the role of such alongshore currents in the transport of nutrients and the subsequent biological effects has rarely

BGD
10, 3891–3923, 2013

been examined, probably because it is commonly believed that the largest gradients both chemically and biologically are only important in the cross-shelf dimension.

Two major continental shelves of the western North Pacific are those of the East China Sea (ECS) and the northern South China Sea (NSCS). The ECS shelf and the NSCS shelf are connected by the Taiwan Strait (TWS) (Fig. 1a) (Chen, 2003, 2008). Hydrographic data characterizes the China Coastal Current (CCC), which is driven by the northeast winter monsoon, to be one of the major water masses in the TWS (Jan et al., 2006, 2010), with relatively low SST ($< 18.0\,^{\circ}C$) and salinity (< 33.0) (Fig. 1a). Chen (2008) reviews the winter nutrient distribution pattern both in the ECS and the TWS and points out the potentially high nutrient fluxes carried by the CCC through the TWS. Based on our new observations together with the available literature data of nutrients and volume transport in the TWS aided by a numerical model, this study sought to quantify such southward nutrient flux and examine its role in sustaining wintertime primary production (PP) on the shelf of the northeast South China Sea (NESCS). We intend to demonstrate that such inter-shelf nutrient flux is a critically important nutrient source sustaining PP on the NESCS shelf in winter, which would be otherwise oligotrophic because of the limited river discharge.

2 Materials and methods

2.1 Study area

The ECS has a broad shelf located in the temperate zone, which is warm (22–28 °C) in summer and cold (~ 9 to 21 °C, Fig. 1a) in winter, especially the inner shelf. The Changjiang River is the largest river emptying into the ECS, with a peak discharge of $50\,000\,m^3\,s^{-1}$ in summer and a minimum of $13\,000\,m^3\,s^{-1}$ in winter (http://xxfb.hydroinfo.gov.cn/). The ECS is influenced by nutrient enriched Changjiang discharge and Kuroshio subsurface water, and has a moderately high PP in summer, ranging ~ 0.2–1.0 $gC\,m^{-2}\,d^{-1}$ (Chen, 1996; Chen and Wang, 1999; Chen et al., 2001;

BGD
10, 3891–3923, 2013

Gong et al., 2003, 2006). However, PP in winter is only one tenth of that in summer probably due to low water temperature and light availability (Gong et al., 2003).

The NSCS has a northeastward widened shelf located in the sub-tropical climate zone with a complicated coastline and topography variations. The water temperature on the shelf is warm in summer (27–28 °C, Han et al., 2012). In winter, the shelf water temperature is lower (18–24 °C, Fig. 1a), but much higher than that in the ECS. The Pearl River is the largest riverine nutrient source to the NSCS shelf with a discharge of 15 500 $m^3 s^{-1}$ in summer and 1800 $m^3 s^{-1}$ in winter (http://xxfb.hydroinfo.gov.cn/). In summer, the coastal upwelling also plays an important role in supplying nutrients (Han et al., 2012). Noteworthy, the PP in the NSCS in winter maintains at similar level as that in summer (~ 0.8–1.0 gC $m^{-2} d^{-1}$, Chen and Chen, 2006; Wang et al., 2012). During this time period, the warm and oligotrophic Kuroshio surface water intrudes and occupies a large area of the NSCS basin (Hu et al., 2000).

The TWS is ~ 180 km wide with an average depth of ~ 60 m (Hong et al., 2011). In winter, the northeast prevailing wind drives the CCC flowing southward. The current is confined within the narrow inner shelf with water depth < 50 m due to the Ekman effect. This coastal current, which originates from the ECS around the Changjiang estuary (Chang and Isobe, 2003; Chen, 2003; Lin et al., 2005; Guan and Fang, 2006), is featured by high concentrations of nutrients as compared with the ambient seawater (Chen, 2003; Gong et al., 2003), primarily owing to the large amount of nutrient input from the Changjiang and wind induced resuspension. The CCC starts in mid-September, peaks from October to January and weakens thereafter, except for some short periods of monsoon wind relaxation or transition (Jan and Chao, 2003; Wu and Hsin, 2005; Lin et al., 2005; Pan et al., 2012).

Although previous studies investigated the circulation and water transport for the entire TWS using a shipboard Acoustic Doppler Current Profiler (sb-ADCP) (Liang et al., 2003; Wang et al., 2003), bottom moored Acoustic Doppler Current Profiler (bm-ADCP) (Lin et al., 2005; Jan et al., 2006), surface drifters (Qiu et al., 2011), high-frequency radar (Zhu et al., 2008) and numerical models (Jan et al., 1998; Wu and Hsin, 2005;

BGD
10, 3891–3923, 2013

Wu et al., 2007; Fang et al., 2009), studies dedicated to the total volume transport of the CCC and its variability and biogeochemical significance have not yet been conducted.

2.2 Sampling and measurements

An expedition on board the R/V *Dongfanghong II* was conducted on the ECS-TWS-NSCS shelves in winter 2008 (from 25 December 2008 to 9 January 2009). Several cross shelf transects covering the region of the ECS and NSCS shelves (marked by PN, 6, 4, 2, A, C; Fig. 1b) were investigated. Most of the sampling stations were located on the shelf (< 200 m isobaths), particularly, at a depth < 50 m along the coastline from the ECS to the NSCS shelf (Fig. 1b).

Samples were taken using Niskin bottles mounted onto a rosette sampler assembly, equipped with a conductivity-temperature-depth (CTD) recorder (Sea-Bird Co., SBE911). Nutrient samples were analyzed using routine spectrophotometric methods with a Technicon AA3 Auto-Analyzer (Bran-Lube, GmbH) (Han et al., 2012 and references therein). The nmol L^{-1} levels of PO_4 were measured according to Ma et al. (2008). Samples for chlorophyll *a* (Chl *a*) were filtered through 25-mm Whatman GF/F glass fiber filters and then were immediately frozen until analysis. These samples were determined using a Turner fluorometer fitted with a red sensitive photomultiplier (Parsons et al., 1984).

2.3 Model description

To better estimate the volume transport of CCC, we adopted the regional ocean modeling system (ROMS) (Shchepetkin and McWilliams, 2005) to simulate the coastal current. ROMS is a free surface, hydrostatic, primitive equation of an ocean model. The Mellor-Yamada 2.5 turbulent sub-model, a bulk-flux formulation for air-sea exchange and benthic boundary layer formulations, is embedded in the ROMS. The model domain was rectangular, extending from 1° N, 99° E in the southwest corner to about 49° N, 143.5° E in the northeast corner with its zonal axis directing eastward and

BGD
10, 3891–3923, 2013

meridional axis northward. The model had an averaged horizontal grid size < 10 km and 30 vertical levels in stretched generalized terrain-following coordinates. The water depths of the model were obtained by merging ETOPO2 (1/30 degree resolution) from the National Geophysical Data Center (USA) with the water depths digitized from navigation maps published by the China's Maritime Safety Administration. The model was forced with 10-yr (1999–2009) monthly mean 1/4 × 1/4 degree QuikSCAT winds and with climatological atmosphere fluxes from the National Centers for Environmental Prediction. Along the southern and eastern open boundaries, climatological momentum and thermal fluxes from the Ocean General Circulation Model for the Earth Simulator (Sasaki et al., 2008) were implemented through the open boundary conditions of Gan and Allen (2005). The model was validated with observed sea surface temperature, dynamic height derived from Archiving, Validation, and Interpretation of Satellite Oceanographic Data and other climatological mean conditions (Gan et al., 2013). The climatological annual transport in the TWS was northward at about 1.1 Sv ($1\,Sv = 10^6\,m^3\,s^{-1}$), close to the estimate of 1.09 Sv by Wu and Hsin (2005) and that of 1.2 Sv by Isobe (2008).

3 Results

3.1 Hydrography

As shown in Fig. 2a and b, a narrow band of water mass with low temperature (~ 12.1–13.0 °C) and low salinity (~ 26.7–31.4) clearly occupied the inner shelf of the ECS in winter. Strong cross shelf gradients in temperature (12.1 to 23.2 °C) and salinity (26.7 to 34.6) were consistent with the satellite SST image during the same period (Fig. 1a). The colder and fresher water mass hugging the coast was the CCC. We also observed an increase in water temperature from ~12.1–16.9 °C while the CCC was flowing southward from the Changjiang estuary mouth through the TWS (Fig. 2a).

BGD
10, 3891–3923, 2013

Meanwhile, a water mass characterized by low temperature (17.5–17.9 °C) and low salinity (~ 32.9–33.0) can be observed in the nearshore region to the east of the Pearl River estuary mouth in the NESCS (Fig. 2a and b). Since there was very limited freshwater discharge from the Pearl River and the wind directed the plume southwestward, such a low temperature and salinity signal was highly likely to have been derived from the extension flow of the CCC. Another water mass with low salinity (~ 31.0) was observed to the west of the Pearl River estuary mouth. This water mass was clearly the Pearl River plume. Away from the inner shelf, the high temperature (~ 21.3–23.7 °C) and high salinity (> 34.0) revealed the influence from the Kuroshio intrusion.

We further used the distributions of field data observed in the ECS (Fig. 3a and b) and the NSCS shelves (Fig. 4a and b) to give a sectional view of the distinctive CCC. At Transect PN (see location in Fig. 1b), the CCC occupied the inner shelf with a water depth mainly < 50 m. Away from the CCC, both temperature and salinity increased gradually and vertically were well mixed as reported previously (Hama et al., 1997; Kim et al., 2009).

At Transect 2 (see location in Fig. 1b) crossing the NSCS shelf, we can see a similar pattern with vertically well mixed colder and lower salinity water nearshore (Fig. 4a and b) except for some downwelling structure which occurred near the bottom layer with cold water (~ 18.0–18.7 °C) extending from the CCC and tilted downward abruptly along the shelf towards offshore (~ 80–100 m isobath) (Fig. 4a). The signal of this downward salinity distribution was weaker than that of the temperature, probably due to fast entrainment with the ambient saline oceanic water (Fig. 4b). A similar pattern is observed by Liu et al. (2010).

3.2 Surface distribution of nutrients and Chl *a*

The surface region occupied by the CCC displayed very high nutrient levels (DIN, PO_4 and $Si(OH)_4$), and waters with the highest nutrient contents (DIN ~ 35.0 µmol L^{-1}, PO_4 ~ 0.89 µmol L^{-1} and $Si(OH)_4$ ~ 38.5 µmol L^{-1}) being located at the southern Changjiang estuary mouth (Fig. 2c–e). The offshore shelf water was characterized by

BGD
10, 3891–3923, 2013

relatively lower nutrients due to the influence of the oligotrophic Kuroshio surface water. However, the nutrient concentrations were still high, for example, 9.6–1.5 μmol L^{-1} for DIN, 0.58–0.15 μmol L^{-1} for PO_4 and 15.4–3.0 μmol L^{-1} for $Si(OH)_4$. Interestingly, although nutrients were abundant over the entire ECS, the Chl *a* values were not concomitantly high (~ 0.3–0.7 mg m^{-3}, see Fig. 2f), probably due to low temperature limitation (Gong et al., 2003).

Compared with the ECS, Chl *a* values in the NSCS shelf were much higher. The Pearl River plume at the southwest had the highest concentrations with values of ~ 14.8 μmol L^{-1} for DIN, ~ 0.51 μmol L^{-1} for PO_4 and ~ 21.9 μmol L^{-1} for $Si(OH)_4$ (Fig. 2c–e) and, correspondingly, high Chl *a* values ~ 1.6 mg m^{-3} could also be observed (Fig. 2f). Nutrients in the NSCS inner shelf were relatively abundant (DIN, PO_4 and $Si(OH)_4$ were ~ 6.6–8.0 μmol L^{-1}, ~ 0.38–0.54 μmol L^{-1} and ~ 10.4–17.6 μmol L^{-1}; see Fig. 2c–e) showing a seaward decreasing pattern. In contrast, the offshore shelf area was characterized by extremely low concentrations in the range < 0.9 μmol L^{-1} for DIN, < 0.12 μmol L^{-1} for PO_4 and < 3.9 μmol L^{-1} for $Si(OH)_4$, reflecting the oligotrophic conditions on the NSCS shelf. Within the ~ 100 m isobath of the NSCS shelf, we see higher values of Chl *a* in the northeastern part (~ 0.6–2.0 mg m^{-3}) relative to those in the southwest (~ 0.4–0.7 mg m^{-3}) indicating extra nutrient supply to stimulate the phytoplankton biomass (Fig. 2f).

3.3 Vertical distribution of nutrients and Chl *a*

Similar to the cross-shelf patterns of temperature and salinity, Transect PN displayed homogeneous features in the nutrients for the whole water column (Fig. 3c–e). The DIN concentration in the nearshore water column could be ~ 9.3–12.5 μmol L^{-1}, but it rapidly decreased seaward to 3.6–7.0 μmol L^{-1} due to the entrainment by oligotrophic Kuroshio water. PO_4 and $Si(OH)_4$ had similar patterns to that of DIN, ranging, respectively, from 0.51–0.68 μmol L^{-1} and ~ 15.1–16.9 μmol L^{-1} in the nearshore to 0.15–0.49 μmol L^{-1} and 3.0–12.3 μmol L^{-1} offshore. The phytoplankton biomass in

BGD
10, 3891–3923, 2013

Transect PN was also homogeneous vertically. It should be noted that the Chl *a* values were relatively low in the CCC ($\sim 0.7\,mg\,m^{-3}$) and on the shelf (~ 0.3–$0.5\,mg\,m^{-3}$) regardless of the high nutrient concentration (Fig. 3f).

Nutrients on the NSCS shelf showed vertical mixing properties in the water column except for the bottom water (Fig. 4c–e). At Transect 2, the nutrient in nearshore water was well mixed vertically, with concentrations of ~ 7.8–$8.0\,\mu mol\,L^{-1}$ for DIN, ~ 0.51–$0.54\,\mu mol\,L^{-1}$ for PO_4, and ~ 16.6–$17.6\,\mu mol\,L^{-1}$ for $Si(OH)_4$. In comparison with the ECS shelf, Chl *a* values were enhanced ($\sim 1.0\,mg\,m^{-3}$) in response to the abundant nutrients (Fig. 4f). Nutrients decreased seaward, with a DIN of $\sim 0.5\,\mu mol\,L^{-1}$, PO_4 of $\sim 0.10\,\mu mol\,L^{-1}$ and $Si(OH)_4$ of $\sim 2.5\,\mu mol\,L^{-1}$, while the corresponding Chl *a* was up to 0.6–0.8 $mg\,m^{-3}$. Nutrients were higher near the bottom around the 30 m isobath (PO_4 $\sim 0.10\,\mu mol\,L^{-1}$ and $Si(OH)_4$ $\sim 3.0\,\mu mol\,L^{-1}$) when compared with those near the upper layer (PO_4 $\sim 0.05\,\mu mol\,L^{-1}$ and $Si(OH)_4$ $\sim 1.7\,\mu mol\,L^{-1}$) due to downwelling nearshore.

The overall hydrological and biogeochemical properties, therefore, showed a clear map of the CCC stream from the ECS shelf to the NSCS shelf in wintertime. To further understand the CCC, detailed nutrient characteristics of the CCC were examined.

3.4 Nutrient characteristics of the CCC

Figure 5 illustrates vertical nutrient profiles from the stations along the CCC pathway. The vertical profiles of nutrients in the CCC stream exhibited a clear decreasing gradient from the ECS shelf to the NSCS shelf via the TWS. For example, for the whole water column, DIN was in the range 24.3–35.7 $\mu mol\,L^{-1}$ in the ECS segment, 2.4–14.1 $\mu mol\,L^{-1}$ in the TWS segment and 2.4–8.0 $\mu mol\,L^{-1}$ in the NSCS segment (Fig. 5a). Spatial variations of PO_4 and $Si(OH)_4$ were similar to those of DIN (Fig. 5b and c), which were highest in the ECS segment but lowest in the NSCS segment.

BGD
10, 3891–3923, 2013

It should also be noted that some point sources from local rivers may add nutrients along the CCC pathway. For example, at Stations F18a and F16 off the Qiantangjiang and Minjiang river mouths, higher concentrations can be seen compared to those at the upstream (Figs. 1b, 2, 5). Such impact from point sources are recognized in previous studies (Wong et al., 2000; Lee and Chao, 2003; Naik and Chen, 2008). However, their contributions are quite limited due to much smaller water discharge in winter (Liu et al., 2009; Yan et al., 2012).

In addition, the nutrient concentrations showed no vertical gradient for those stations with water depth < 30 m. In contrast, for stations deeper than 30 m, surface nutrient concentrations were considerably higher than that at the bottom. For example, the surface nutrients in the TWS segment, at Station F15 (14.1 $\mu mol\,L^{-1}$ for DIN, 0.57 $\mu mol\,L^{-1}$ for PO_4, and 15.9 $\mu mol\,L^{-1}$ for $Si(OH)_4$), were much higher than those of the bottom waters (2.6 $\mu mol\,L^{-1}$ for DIN, 0.19 $\mu mol\,L^{-1}$ for PO_4, and 3.6 $\mu mol\,L^{-1}$ for $Si(OH)_4$). As expected, nutrient structures in the CCC which was obtained in winter 2009 had a similar distribution (Dai, unpublished data, not shown) compared to those in winter 2008. However, nutrients in winter 2009 displayed features of highly vertical mixing. For example, nutrients at the same Station F15 were almost identical between the two winters in the surface layer but much higher in the bottom layer during winter 2009 (9.3 $\mu mol\,L^{-1}$ for DIN, 0.51 $\mu mol\,L^{-1}$ for PO_4 and 10.1 $\mu mol\,L^{-1}$ for $Si(OH)_4$). The elevated nutrient concentration in the bottom may be induced either from the particle re-mineralization in the water column or regeneration from the sediment (Kao et al., 2003; Liu et al., 2007).

We also calculated the mean nutrient concentration for the water column at each station (Fig. 5d) along the CCC. For example, the variations of averaged depth-integrated DIN (IDIN) largely followed the surface distributions (Fig. 2), demonstrating a southward decreasing gradient with latitude (from ~ 40.0 to < 5.0 $\mu mol\,L^{-1}$). Similar patterns of averaged depth-integrated PO_4 and $Si(OH)_4$ could also be seen (not shown).

Zooming into the TWS segment (Station F15) (Fig. 1c), averaged IDIN concentrations were ~ 8.9–13.1 $\mu mol\,L^{-1}$ in the two winter seasons (2008 and 2009). Previous results from field observation were shown here for comparison. Average nitrate in the

BGD
10, 3891–3923, 2013

TWS (from ~24.2° N, 118.5° E to ~26.2° N, 120.4° E) range ~13.0–15.0 μmol L^{-1} in January, 2003 (Chen, 2008; Naik and Chen, 2008). Average nitrate concentration in the northern TWS (~25.3° N, 120.0° E) decreased from ~14.0 μmol L^{-1} in the surface to ~4.0 μmol L^{-1} in the bottom in March, 1997 (Liu et al., 2000). In addition, DIN concentrations in the southern TWS (~24.4° N, 118.7° E) were ~7.7–20.1 μmol L^{-1} in November, 2008 (Yan, 2011). Taken together, there was no noticeable inter-winter variation in DIN concentrations in the CCC of the TWS segment. Considering the vertical variation, it was reasonable to use the averaged depth-integrated concentration of ~11.0 ± 2.0 μmol L^{-1} to represent the DIN level in the CCC of the TWS segment.

To further characterize the nutrients in the CCC, the relationships between DIN and PO_4, and $Si(OH)_4$ and DIN in winter were constructed (Fig. 6a and b). In detail, the DIN : PO_4 ratio in the CCC was ~33.8, remarkably lower than that in the Changjiang (~100–160 : 1) (Liu et al., 2009). The rapid reduction of the DIN : PO_4 ratio from the Changjiang to the CCC might primarily be due to a combination of biological consumption and the mixing with the ambient seawater with low DIN : PO_4 ratios (Chai et al., 2006; Zhang et al., 2007; Lui and Chen, 2011). Differing from the CCC, the ECS and the NSCS shelf waters were characterized by low DIN : PO_4 ratios of ~14.9, consistent with the ratios in oceanic water (Wong et al., 2007). Similarly, the DIN : PO_4 ratio in the Pearl River plume was close to that of the CCC, being ~32 : 5 (Fig. 6a). The ratio was much lower than that in the Pearl River (~50–100 : 1) (Dai et al., 2013), primarily due to the same mechanisms as that for the CCC.

$Si(OH)_4$: DIN ratios in the different water masses were generally close to ~1 : 1 (Fig. 6b). The ratios in the CCC and Pearl River plume appeared to be resulted from silicate chemical weathering within the river basin (Zhao, 1990; Chetelat et al., 2008). In the ECS and NSCS shelf, the ratios between $Si(OH)_4$ and DIN also appeared to be ~1 : 1. This might be due to particle re-mineralization, which leads to the release of $Si(OH)_4$ and DIN in the water column with a molar ratio of ~1 : 1 (Redfield et al., 1963; Koike et al., 2001).

BGD
10, 3891–3923, 2013

In summary, a closer look at the CCC revealed that the hydrographic characteristics of the CCC were distinctly different from those of the shelf water. This nutrient-enriched CCC was primarily sourced from the ECS and was interconnected with the ECS shelf and the NSCS shelf via the western TWS.

3.5 Potential nutrient sources supporting phytoplankton biomass on the NESCS shelf

In order to further examine algae biomass over the shelf, long-term MODIS Chl *a* in winter was used (Fig. 7a). Since the satellite-derived Chl *a* concentration is not sufficient to represent the nearshore phytoplankton biomass due to the impact from the high suspended particle concentration (Kiyomoto et al., 2001; Liu et al., 2007), we only focused on the shelf area beyond the nearshore. Figure 7a shows that MODIS Chl *a* in the NESCS shelf ranged from ~ 0.5 to $2.5\,mg\,m^{-3}$, which was consistent with our field observations (Fig. 2f), suggesting that the high phytoplankton biomass occurred on the NESCS shelf was common during the wintertime.

In addition, to explore the algae biomass of the entire water column on the ECS and NESCS shelves, averaged integrated Chl *a* (IChl *a*) concentrations were calculated and assembled in Fig. 7b. Averaged IChl *a* concentrations on the inner and middle ECS shelf were as low as 0.5 ± 0.2 and $0.4 \pm 0.1\,mg\,m^{-3}$, respectively, and were probably limited by the low temperature as mentioned above (Gong et al., 2003). In contrast, higher averaged IChl *a* concentrations were found on the inner and middle NESCS shelf, being 1.3 ± 0.7 and $1.0 \pm 0.4\,mg\,m^{-3}$. Recent studies also find that the NSCS shelf have high new production (NP) of ~ 0.15–$0.34\,gC\,m^{-2}\,d^{-1}$ in wintertime (Chen and Chen, 2006; Wang et al., 2012), which is almost comparable to that in summer (~ 0.06–$0.17\,gC\,m^{-2}\,d^{-1}$, Chen and Chen, 2006).

On the contrary, in winter, DIN flux is $\sim 200\,mol\,s^{-1}$ around the Pearl River estuary (Liu et al., 2009). In addition, the Pearl River plume flows southwestward driven by the northeast monsoon (Ou et al., 2009), and such Pearl River DIN input was not able to sustain high phytoplankton biomass in the NESCS. Moreover, coastal upwelling was

BGD
10, 3891–3923, 2013

displaced by the downwelling in winter which could transport nutrients towards the offshore area along the steep slope (Liu et al., 2010; Gan et al., 2012). Furthermore, nutrients on the NSCS shelf might also be diluted by the oligotrophic Kuroshio surface water (Chen et al., 2010). Altogether, nutrient-enriched CCC should be the important external nutrient sources transported to the NESCS shelf and to support the high phytoplankton biomass which has so far not received much attention. Coupling the field DIN observation with the CCC volume transport, it was possible to quantify the DIN flux transported by the CCC (see following discussion).

4 Discussion

4.1 CCC volume transport across the western TWS

4.1.1 Field observations

During October–December 1999 and January–February 2001, along-strait current velocities in the western TWS were measured using a bm-ADCP (Fig. 1c). Volume transport of the CCC was calculated by multiplication between the integrated de-tided current velocity from the sea surface to the bottom and a coastal width of ~ 30 km (to $\sim 119.2^{\circ}$ E). Figure 8a and b show that the total volume transport (T_T calculated in Sv units) displayed a different flowing direction and different amplitude, driven by the different wind stress and the consequent pressure gradient forcing (Wu and Hsin, 2005). In winter 1999, T_T varied from -1.08 to 0.50 Sv, with an average negative value (southward) of -0.35 ± 0.26 Sv and a positive value (northward) of 0.12 ± 0.11 Sv (Fig. 8a). Net T_T was calculated to be -0.23 Sv. The T_T in winter 2001 followed a similar pattern to that in winter 1999, but had lower values ranging from -0.59 to 0.43 Sv (Fig. 8a), primarily due to the weaker wind stress ($\sim 15\,m\,s^{-1}$ in winter 1999 and $\sim 11\,m\,s^{-1}$ in winter 2001). Based on the average negative value -0.19 ± 0.14 Sv and the positive value 0.13 ± 0.10 Sv, the net T_T was calculated to be -0.07 Sv.

BGD
10, 3891–3923, 2013

In addition, Liang et al. (2003), using sb-ADCP to measure the current velocity in the TWS in winter, find values ranging from ~ -0.1 to $-0.2\,m\,s^{-1}$ in the west of the TWS (25.0° N, ~ 119.0–119.5° E). If we assumed the water depth was 20 m, and the coastal width ~ 54 km (see Fig. 16 in Liang et al., 2003), the southward T_T could then be estimated to be ~ 0.1–0.2 Sv. Moreover, the lower T_T around 25.27° N and 119.98° E was estimated to be ~ 0.05 Sv, dependent on the $\sim 0.05\,m\,s^{-1}$ southward current velocity, the ~ 30 m average water depth and the ~ 30 km coastal width (to ~ 119.7° E) (Fu et al., 1991). Around the same location and assuming the consistent wind speed, the T_T was ~ 0.06–0.12 Sv based on the $\sim 0.1–0.2\,m\,s^{-1}$ southwestward velocity which was measured using bm-ADCP (Pan et al., 2012).

In summary, the southward T_T could range from ~ 0.05–0.23 Sv based on different observation results of current field (Table 1).

4.1.2 Model results

Considering that the field observations in the TWS were generally short-term, and especially with limited spatial and temporal coverage, a climatological numerical model was adopted to simulate the current velocity across the TWS in the entire winter (December, January and February).

Figure 9 shows the modeled climatological along-shore current velocity along 24.6° N across the TWS in winter. The model-derived velocity structure exhibited two segments: one was the southward CCC, which was constrained in the nearshore of Mainland China; the other was the northward SCS water and Kuroshio water, located in the eastern TWS. Such a pattern was consistent with previous results from in situ observations, supporting the validity of our numerical model (Fu et al., 1991; Liang et al., 2003; Chen et al., 2010).

To further validate our climatological model, the modeled current velocity at Station F15 (24.6° N and 119.0° E) was chosen to compare with that at Station WC1 with in situ observation, as they shared a similar location (Fig. 1c) and wind speed ($\sim 11\,m\,s^{-1}$).

BGD
10, 3891–3923, 2013

The modeled velocity of the CCC at Station F15 decreased gradually from 0.29 m s^{-1} at the surface to < 0.1 m s^{-1} at the bottom, and the resulted average depth-integrated velocity was 0.06 m s^{-1} (Fig. 9). Assuming uniform velocities across the section with the ~ 25–44 m water depth and the ~ 17.5 km coastal width (to ~ 118.84° E), the integrated T_T could be estimated to be ~ 0.04 Sv, which was consistent with the results derived from Station WC1 (0.07 Sv). Such a validation suggested that our model was robust enough to reproduce the physical dynamics of the CCC.

Model-derived T_T also displays another important feature that a zonal current velocity gradient existed in the CCC (Fig. 9). The velocity essentially decreased from ~ 0.3 m s^{-1} in the nearshore area to 0.1 m s^{-1} in the offshore region within CCC. Such a pattern was validated by previous sb-ADCP measurements surveyed around a similar location (Liang et al., 2003). If we integrated the modeled current velocity between nearshore and Station F15 (118.84–119.0° E, ~ 17.5 km), the average velocity could then be modified as 0.17 m s^{-1}, and the T_T was further estimated to be 0.13 Sv.

In summary, our estimates based on both the direct measurement and numerical model approaches were consistent and the integrated T_T of 0.13 Sv was more reasonable to represent the winter CCC T_T level in the TWS.

4.2 DIN flux by CCC

The DIN flux of the CCC across the TWS could be derived from simple multiplication between the average DIN concentration and the average T_T. As mentioned above, the average DIN in the CCC across the TWS was ~ 11.0 ± 2.0 µmol L^{-1}. Based on the modeled T_T, being 0.13 Sv, which represented the whole transectional CCC volume transport, the DIN flux was estimated to be ~ 1430 ± 260 mol s^{-1}.

In comparison, the wintertime DIN flux was ~ 760 mol s^{-1} around the Changjiang estuary mouth (Liu et al., 2009). The CCC associated DIN flux was therefore equivalent to ~ 2 times that from the Changjiang or ~ 7 times that from the Pearl River.

BGD
10, 3891–3923, 2013

The fact that the DIN flux transported by the CCC was larger than that of the Changjiang nutrient discharge simply reflected that there were additional nutrient sources. Similar results were found for the PO_4 flux based on the DIN : PO_4 ratios in the CCC and the PO_4 flux in the Changjiang estuary mouth (Liu et al., 2009). Possible sources of these nutrients may include nutrient regeneration during the CCC pathway and nutrient transported offshore (Chen and Wang, 1999; Zhu et al., 2006).

4.3 CCC-supported "new production" on the NESCS shelf

Assuming winter lasts from December to February, the total DIN transported by the CCC was calculated to be $\sim 11.1 \pm 2.0 \times 10^9$ mol N. If we assumed C : N ratio of 106 : 16, this amount of DIN would be equivalent to $\sim 8.8 \pm 1.6 \times 10^{11}$ gC being fixed on the NESCS shelf. Our parallel study based on the same cruise in winter 2008, the NP and the PP at Station S608 (see location in Fig. 1b, water depth ~ 106–118 m, or Station S1 in Wang et al., 2012) on the NESCS shelf have been measured to be about 0.15 gC m^{-2} d^{-1} and 0.51 gC m^{-2} d^{-1} (Wang et al., 2012). In addition, the NP and the PP at one station located around 73 m deep on the NESCS shelf in winter 2004 have been reported to be about 0.34 gC m^{-2} d^{-1} and 0.82 gC m^{-2} d^{-1} (Chen and Chen, 2006), slightly higher than that in winter 2008. Furthermore, a consistent estimate of winter PP being ~ 0.8 gC m^{-2} d^{-1} was given by Hao et al. (2007) for the inner NESCS shelf. In this study for the purpose of first order estimation, we adopted the range of an NP of ~ 0.15–0.34 gC m^{-2} d^{-1} and a PP of ~ 0.51–0.82 gC m^{-2} d^{-1}. Given that the surface area of NESCS shelf shallower than ≤ 100 m is $\sim 5 \times 10^4$ km^2 (from Google Earth Pro software), we estimated that the CCC-associated DIN supported ~ > 58 ± 10 % of NP and ~ 38 ± 7–24 ± 4 % of PP.

BGD
10, 3891–3923, 2013

5 Concluding remarks

This study has highlighted that the monsoonal wind-driven CCC might be a primary conduit for nutrient transport between the ECS and the NSCS shelf. Our estimate has shown that the DIN flux carried by the CCC across the TWS was $\sim 1430 \pm 260\,\mathrm{mol\,s^{-1}}$, ~ 2 times that from the Changjiang or ~ 7 times that from the Pearl River in winter. It is important to emphasize that nutrients escaped from the cold and relatively nutrient enriched ECS shelf may significantly stimulate PP in the NESCS shelf where the water temperature remained warm in winter which was thus favorable for biological production. Our first order estimation indeed showed that the DIN input flux carried by the CCC might support a carbon fixation of $\sim 8.8 \pm 1.6 \times 10^{11}$ gC on the NESCS shelf, representing $\sim > 58 \pm 10\,\%$ of the NP and $\sim 38 \pm 7\text{-}24 \pm 4\,\%$ of the PP therein.

Acknowledgements. This research was funded by the National Basic Research Program of China (973 Program) through grant 2009CB421204 and 2009CB421201. We thank X. Huang, and J. Yang for their help with ancillary data and sample collection. We are grateful to L. Liang for the help in the modeling work. Author SJ calculated the flow volume transport using the current velocity profile data collected during Taiwan Strait Nowcast (TSNOW) project with the collaboration of T. Y. Tang of NTU and S.-F. Lin of ITRI. We also thank the crew of R/V *Dongfanghong II* for their cooperation during the cruise. We thank K.-K. Liu for his constructive suggestions and J. Hodgkiss for his help with English.

References

Chai, C., Yu, Z., Song, X., and Cao, X.: The status and characteristics of eutrophication in the Yangtze River (Changjiang) Estuary and the adjacent East China Sea, China, Hydrobiologia, 563, 313–328, 2006.

Chang, P.-H. and Isobe, A.: A numerical study on the Yangtze diluted water in the Yellow and East China Seas, J. Geophys. Res., 108, 3299, doi:10.1029/2002JC001749, 2003.

Chen, C.-T. A.: The Kuroshio intermediate water is the major source of nutrients on the East China Sea continental shelf, Oceanol. Acta, 19, 523–527, 1996.

BGD
10, 3891–3923, 2013

Chen, C.-T. A. and Wang, S.-L.: Carbon, alkalinity and nutrient budgets on the East China Sea continental shelf, J. Geophys. Res., 104, 20675–20686, 1999.
Chen, C.-T. A.: Rare northward flow in the Taiwan Strait in winter: A note, Conti. Shelf Res., 23, 387–391, 2003.
Chen, C.-T. A.: Distributions of nutrients in the East China Sea and the South China Sea connection, J. Oceanogr., 64, 737–751, 2008.
Chen, C.-T. A., Jan, S., Huang, T.-H., and Tseng, Y.-H.: Spring of no Kuroshio intrusion in the southern Taiwan Strait, J. Geophys. Res., 115, C08011, doi:08010.01029/02009JC005804, 2010.
Chen, Y.-l. L., Chen, H.-Y., Lee, W.-H., Hung, C.-C., Wong, G. T. F., and Kanda, J.: New production in the East China Sea, comparison between well-mixed winter and stratified summer conditions, Conti. Shelf Res., 21, 751–764, 2001.
Chen, Y.-l. L. and Chen, H.-Y.: Seasonal dynamics of primary and new production in the northern South China Sea: The significance of river discharge and nutrient advection, Deep-Sea Res. I, 53, 971–986, 2006.
Chetelat, B., Liu, C.-Q., Zhao, Z., Wang, Q., Li, S., Li, J., and Wang, B.: Geochemistry of the dissolved load of the Changjiang Basin rivers: Anthropogenic impacts and chemistry weathering, Geochim. et Cosmochim. Ac., 72, 4254–4277, 2008.
Dai, M., Gan, J., Han, A., Kung, H., and Yin, Z.: Physical Dynamics and Biogeochemistry of the Pearl River Plume, in: Biogeochemical Dynamics at Large River-Coastal Interfaces: Linkages with Global Climate Change, edited by: Bianchi, T., Allison, M., and Cai, W., chapter 13, Cambridge University Press, accepted, 2013.
Fang, G., Wang, Y., Wei, Z., Fang, Y., Qiao, F., and Hu, X.: Interocean circulation and heat and freshwater budgets of the South China Sea based on a numerical model, Dynam. Atmos. Oceans, 47, 55–72, 2009.
Fu, Z., Hu, J., and Yu, G.: Seawater flux through Taiwan Strait, Chin. J. Oceanol. Limn., 9, 232–239, 1991.
Gan, J. and Allen, J. S.: On open boundary conditions for a limited-area coastal model off Oregon, Pt 1, Response to idealized wind forcing, Ocean Model., 8, 115–133, doi:10.1016/j.ocemod.2003.12.006, 2005.
Gan, J., Ho, H. S., and Liang, L.: Dynamics of intensified downwelling circulation over a widened shelf, J. Phys. Oceanogr., 43, 80–94, doi:10.1175/JPO-D-12-02.1, 2012.

BGD
10, 3891–3923, 2013

Gong, G.-C., Wen, Y.-H., Wang, B.-W., and Liu, G.-J.: Seasonal variation of chlorophyll *a* concentration, primary production and environmental conditions in the subtropical East China Sea, Deep-Sea Res. II, 50, 1219–1236, 2003.

Gong, G.-C., Chang, J., Chiang, K.-P., Hsiung, T.-M., Hung, C.-C., Duan, S.-W., and Codispoti, L. A.: Reduction of primary production and changing of nutrient ratio in the East China Sea: Effect of the Three Gorges Dam?, Geophys. Res. Lett., 33, L07610, doi:10.1029/2006GL025800, 2006.

Gong, G.-C., Liu, K.-K., Chiang, K.-P., Hsiung, T.-M., Chang, J., Chen, C.-C., Hung, C.-C., Chou, W.-C., Chung, C.-C., Chen, H.-Y., Shiah, F.-K., Tsai, A.-Y., Hsieh, C.-h., Shiao, J.-C., Tseng, C.-M., Hsu, S.-C., Lee, H.-J., Lee, M.-A., Lin, I.-I., and Tsai, F.: Yangtze River floods enhance coastal ocean phytoplankton biomass and potential fish production, Geophys. Res. Lett., 38, L13603, doi:10.1029/2011GL047519, 2011.

Guan, B. and Fang, G.: Winter counter-wind currents off the southeastern China coast: A review, J. Oceanogr., 62, 1–24, 2006.

Guo, X., Zhu, X.-H., Wu, Q.-S., and Huang, D.: The Kuroshio nutrient stream and its temporal variation in the East China Sea, J. Geophys. Res., 117, C01026, doi:10.1029/2011JC007292, 2012.

Hama, T., Shin, K. H., and Handa, N.: Spatial variability in the primary productivity in the East China Sea and its adjacent waters, J. Oceanogr., 53, 41–51, 1997.

Han, A., Dai, M., Kao, S.-J., Gan, J., Li, Q., Wang, L., Zhai, W., and Wang, L.: Nutrient dynamics and biological consumption in a large continental shelf system under the influence of both a river plume and coastal upwelling, Limnol. Oceanogr., 57, 486–502, 2012.

Hao, Q., Ning, X., Liu, C., Cai, Y., and Le, F.: Satellite and in situ observations of primary production in the northern South China Sea, Acta Oceanol. Sin., 29, 58–68, 2007. (in Chinese)

Hong, H., Chai, F., Zhang, C., Huang, B., Jiang, Y., and Hu, J.: An overview of physical and biogeochemical processes and ecosystem dynamics in the Taiwan Strait, Cont. Shelf Res., 31, 3–12, 2011.

Hu, J., Kawamura, H., Hong, H., and Qi, Y.: A review on the currents in the South China Sea: Seasonal circulation, South China Sea warm current and Kuroshio intrusion, J. Oceanogr., 56, 607–624, 2000.

Isobe, A.: Recent advances in ocean-circulation research on the Yellow Sea and East China Sea shelves, J. Oceanogr., 64, 569–584, 2008.

BGD
10, 3891–3923, 2013

Jan, S., Chern, C.-S., and Wang, J.: A numerical study of currents in the Taiwan Strait during winter, Terr. Atmos. Ocean. Sci., 9, 615–632, 1998.
Jan, S., Wang, J., Chern, C.-S., and Chao, S.-Y.: Seasonal variation of the circulation in the Taiwan Strait, J. Marine Syst., 35, 249–268, 2002.
Jan, S. and Chao, S.-Y.: Seasonal variation of volume transport in the major inflow region of the Taiwan Strait: the Penghu Channel, Deep-Sea Res. II, 50, 1117–1126, 2003.
Jan, S., Sheu, D. D., and Kuo, H.-M.: Water mass and throughflow transport variability in The Taiwan Strait, J. Geophys. Res., 111, C12012, doi:10.1029/2006JC003656, 2006.
Jan, S., Tseng, Y.-H., and Dietrich, D. E.: Sources of water in the Taiwan Strait, J. Oceanogr., 66, 211–221, 2010.
Kao, S.-J., Lin, F.-J., and Liu, K.-K.: Organic carbon and nitrogen contents and their isotopic compositions in surficial sediments from the East China Sea shelf and the southern Okinawa Trough, Deep-Sea Res. II, 50, 1203–1217, 2003.
Keafer, B. A., Churchill, J. H., Jr., D. J. M., and Anderson, D. M.: Bloom development and transport of toxic *Alexandrium fundyense* populations within a coastal plume in the Gulf of Maine, Deep-Sea Res. II, 52, 2674–2697, 2005.
Kim, D., Choi, S. H., Kim, K. H., Shim, J., Yoo, S., and Kim, C. H.: Spatial and temporal variations in nutrient and chlorophyll-*a* concentrations in the northern East China Sea surrounding Cheju Island, Cont. Shelf Res., 29, 1426–1436, 2009.
Kiyomoto, Y., Iseki, K., and Okamura, K.: Ocean color satellite imagery and shipboard measurements of chlorophyll *a* and suspended particulate matter distribution in the East China Sea, J. Oceanogr., 57, 37–45, 2001.
Koike, I., Ogawa, H., Nagata, T., Fukuda, R., and Fukuda, H.: Silicate to nitrogen ratio of the upper Sub-Arctic Pacific and the Bering Sea Basin in summer: Its implication for phytoplankton dynamics, J. Oceanogr., 57, 253–260, 2001.
Ladd, C., Stabeno, P., and Cokelet, E. D.: A note on cross-shelf exchange in the northern Gulf of Alaska, Deep-Sea Res. II, 52, 667–679, 2005.
Lee, H.-J., and Chao, S.-Y.: A climatological description of circulation in and around the East China Sea, Deep-Sea Res. II, 50, 1065–1084, 2003.
Liang, W.-D., Tang, T., Yang, Y., Ko, M., and Chuang, W.-S.: Upper-ocean currents around Taiwan, Deep-Sea Res. II, 50, 1085–1105, 2003.
Lin, S., Tang, T., Jan, S., and Chen, C.-J.: Taiwan Strait current in winter, Cont. Shelf Res., 25, 1023–1042, 2005.

BGD
10, 3891–3923, 2013

Liu, J., Xu, K., Li, A., Milliman, J. D., Velozzi, D. M., Xiao, S., and Yang, Z.: Flux and fate of Yangtze River sediment delivered to the East China Sea, Geomorphology, 85, 208–224, 2007.

Liu, K.-K., Tang, T., Gong, G.-C., Chen, L.-Y. L., and Shiah, F.-K.: Cross-shelf and along-shelf nutrient fluxes derived from flow fields and chemical hydrography observed in the southern East China Sea off northern Taiwan, Cont. Shelf Res., 20, 493–523, 2000.

Liu, S. M., Hong, G.-H., Zhang, J., Ye, X. W., and Jiang, X. L.: Nutrient budgets for large Chinese estuaries, Biogeosciences, 6, 2245–2263, doi:10.5194/bg-6-2245-2009, 2009.

Liu, S., Guo, X., Chen, Q., Zhang, J., Bi, Y., Luo, X., and Li, J.: Nutrient dynamics in the winter thermohaline frontal zone of the northern shelf region of the South China Sea, J. Geophys. Res., 115, C11020, doi:11010.11029/12009JC005951, 2010.

Lui, H.-K., and Chen, C.-T. A.: Shifts in limiting nutrients in an estuary caused by mixing and biological activity, Limnol. Oceanogr., 56, 989–998, 2011.

Ma, J., Yuan, D., and Liang, Y.: Sequential injection analysis of nanomolar soluble reactive phosphorus in seawater with HLB solid phase extraction, Mar. Chem., 111, 151–159, 2008.

Naik, H. and Chen, C.-T. A.: Biogeochemical cycling in the Taiwan Strait, Estuar. Coast. Shelf S., 78, 603–612, 2008.

Ou, S., Zhang, H., and Wang, D.: Dynamics of the buoyant plume off the Pearl River Estuary in summer, Environ. Fluid Mech., 9, 471–492, 2009.

Pan, A., Wan, X., Guo, X., and Jing, C.: Responses of the Zhe-Min coastal current adjacent to Pingtan Island to the wintertime monsoon relaxation in 2006 and its mechanism, Sci. China Ser. D., 42, 1317–1328, 2012.

Parsons, T. R., Maita, Y., and Lalli, C. M.: A manual of chemical and biological methods for seawater analysis, Pergamon, 1984.

Qiu, Y., Li, L., Chen, C.-T. A., Guo, X., and Jing, C.: Currents in the Taiwan Strait as observed by surface drifters, J. Oceanogr., 67, 395–404, 2011.

Redfield, A. C., Ketchum, B. H., and Richards, F. A.: The influence of organisms on the composition of seawater, in: The Sea, edited by: Hill, M. N., John Wiley, New York, 2, 26–77, 1963.

Sasaki, H., Nonaka, M., Masumoto, Y., Sasai, Y., Uehara, H., and Sakuma, H.: An eddy-resolving hindcast simulation of the quasi global ocean from 1950 to 2003 on the Earth Simulator, in: High Resolution Numerical Modelling of the Atmosphere and Ocean, edited by: Hamilton, K. and Ohfuchi, W., chapter 10, 157–185, Springer, New York, 2008.

BGD
10, 3891–3923, 2013

Shchepetkin, A. F. and McWilliams, J. C.: The regional oceanic modeling system (ROMS): A split-explicit, free-surface, topography-following-coordinate oceanic model, Ocean Model., 9, 437–404, 2005.

Sugimoto, R., Kasai, A., Miyajima, T., and Fujita, K.: Transport of oceanic nitrate from the continental shelf to the coastal basin in relation to the path of the Kuroshio, Cont. Shelf Res., 29, 1678–1688, 2009. (in Chinese)

Wang, L., Lin, L., Xie, Y., and Huang, B.: A preliminary study on the new productivity and primary productivity of East China Sea and northern South China Sea in winter, J. Mar. Sci., 30, 59–66, 2012.

Wang, Y. H., Jan, S., and Wang, D. P.: Transports and tidal current estimates in the Taiwan Strait from shipboard ADCP observations (1999–2001), Estuar. Coast. Shelf S., 57, 193–199, 2003.

Whitney, F. A., Crawford, W. R., and Harrison, P. J.: Physical processes that enhance nutrient transport and primary productivity in the coastal and open ocean of the subarctic NE Pacific, Deep-Sea Res. II, 52, 681–706, 2005.

Wollast, R.: The coastal organic carbon cycle: Fluxes, sources, and sinks, Ocean Margin Processes in Global Change, edited by: In: Mantoura, R. F. C., Martin, J. M., and Wollast, R., Wiley, New York, 365–381, 1991.

Wollast, R.: Interactions of carbon and nitrogen cycles in the coastal zone, in: Interactions of C, N, P and S biogeochemical cycles and global change, edited by: Wollast, R., Mackenzie, F. T., and Chou, L., Springer, Berlin, 195–210, 1993.

Wong, G. T. F., Chao, S.-Y., Li, Y.-H., and Shiah, F.-K.: The Kuroshio edge exchange process (KEEP) study-an introduction to hypotheses and highlights, Cont. Shelf Res., 20, 335–347, 2000.

Wong, G. T. F., Tseng, C.-M., Wen, L.-S., and Chung, S.-W.: Nutrient dynamics and N-anomaly at the SEATS station, Deep-Sea Res. II, 54, 1528–1545, 2007.

Wu, C.-R. and Hsin, Y.-C.: Volume transport through the Taiwan Strait: A numerical study, Terr. Atmos. Ocean. Sci., 16, 377–391, 2005.

Wu, C.-R., Chao, S.-Y., and Hsu, C.: Transient, seasonal and interannual variability of the Taiwan Strait current, J. Oceanogr., 63, 821–833, 2007.

Yan, X.: Distribution, decadal changes and fluxes of dissolved nutrients in the Jiulong River Estuary, Southwestern Taiwan Strait, M. S., thesis, Xiamen University, China, 40 pp., 2011.

BGD
10, 3891–3923, 2013

Yan, X., Zhai, W., Hong, H., Li, Y., Guo, W., and Huang, X.: Distribution, fluxes and decadal changes of nutrients in the Jiulong River Estuary, Southwest Taiwan Strait, Chinese Sci. Bull., 57, 2307–2318, 2012. (in Chinese)

Zhang, J., Liu, S., Ren, J., Wu, Y., and Zhang, G.: Nutrient gradients from the eutrophic Changjiang (Yangtze River) Estuary to the oligotrophic Kuroshio waters and re-evaluation of budgets for the East China Sea Shelf, Prog. Oceanogr., 74, 449–478, 2007.

Zhao, H.: Evolution of the Pearl River Estuary, Ocean Press, Beijing, 357, 1990. (in Chinese)

Zhu, D., Li, L., Li, Y., and Guo, X.: Seasonal variation of surface currents in the southwestern Taiwan Strait observed with HF radar, Chinese Sci. Bull., 53, 2385–2391, 2008.

Zhu, Z., Zhang, J., Wu, Y., and Lin, J.: Bulk particulate organic carbon in the East China Sea: Tidal influence and bottom transport, Prog. Oceanogr., 69, 37–60, 2006.

BGD
10, 3891–3923, 2013

Table 1. Summary of basic information of the China Coastal Current.

Velocity ($m\,s^{-1}$)	Distance (km)	Depth (m)	Location	T_T (Sv)	Refs.
−0.1 ~ −0.2	~ 119.0–119.5° E; 54	20	25.0° N, ~ 119.0–119.5° E	−0.1 ~ −0.2	Liang et al. (2003)
−0.19	119.20–119.47° E 30	40	C1, 24.96° N, 119.47° E	−0.23	Obs. in 1999, this study
−0.05	119.21–119.49° E 30	40	WC1, 24.80° N, 119.49° E	−0.07	Obs. in 2001, this study
−0.05	119.7–119.98° E 30	30	25.27° N, 119.98° E	−0.05	Fu et al. (1991)
−0.1 ~ −0.2	119.7–119.98° E 30	20	25.27° N, 119.98° E	−0.06 ~ −0.12	Pan et al. (2012)
−0.06	118.84–119.0° E 17.5	25–44	24.6° N, 119.0° E	−0.04	Model result, this study
−0.17	area integration 17.5	25–44	24.6° N, 118.84–119.0° E	−0.13	Model result, this study

BGD
10, 3891–3923, 2013

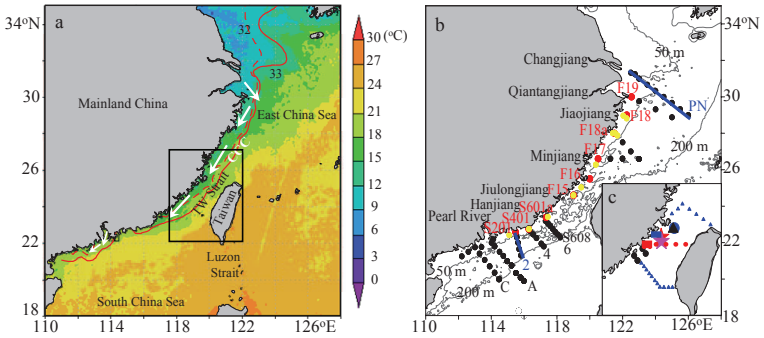

Fig. 1. (a) Map of the study area showing the East China Sea (ECS), the northern South China Sea (NSCS) as well as the Taiwan Strait (TWS). Red curves represented the schematic isohalines of the CCC in winter according to winters 2008 (this study) and 2009 (Dai, unpublished data). The color background represented the mean sea surface temperature (SST) over December–February 2008. SST image was sourced from http://gdata1.sci.gsfc.nasa.gov/daac-bin/G3/gui.cgi?instance_id = ocean_month&selectedMap = Blue%20Marble&. Schematic CCC, river plume of Changjiang and Pearl River were marked by white arrows (Jan et al., 2002; Guan and Fang, 2006; Chen, 2003, 2008; Ou et al., 2009). **(b)** Map of the cruise track and sampling stations (black dots) in winter 2008. Red and yellow dots represented sampling stations within the CCC regime in winters 2008 and 2009, respectively. Transect PN in the ECS and Transect 2 on the NSCS shelf were highlighted by blue lines. The 50 m and 200 m isobaths were also shown. **(c)** In the TWS, blue triangles, black dots and blue dots represented the stations sampled in January 2003 by Naik and Chen (2008), in November 2008 by Yan (2011) and in March 1997 by Liu et al. (2000), respectively. The locations where bottom mounted-ADCP deployments were marked by pink star for Site WC1 in September–December 1999 and by red star for Site C1 deployed in January–February 2001. The black triangle located in the TWS refers to the study site of Fu et al. (1991). The horizontal blue line in the western TWS marked the coastal width for volume transport estimation based on the bm-ADCP. The red line across the TWS was the transect which was adopted to estimate the current velocity from climatological numerical model (the solid one in the western part indicated the southward CCC in the model).

BGD
10, 3891–3923, 2013

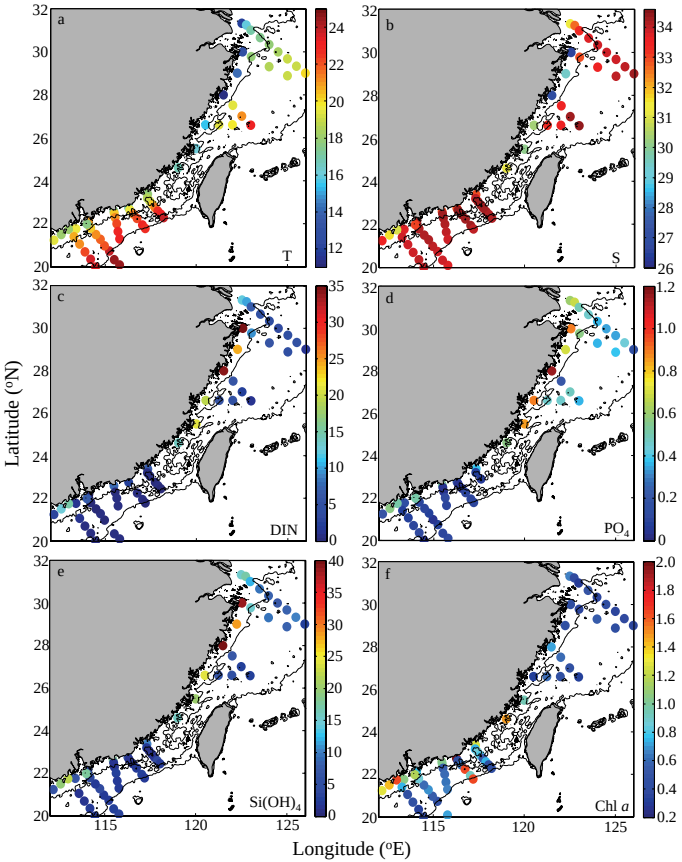

Fig. 2. Surface distributions of temperature (T) (**a**, °C), salinity (**b**, S), DIN ($NO_3 + NO_2$) (**c**, μmol L^{-1}), PO_4 (**d**, μmol L^{-1}), $Si(OH)_4$ (**e**, μmol L^{-1}) and Chl a (**f**, mg m^{-3}) on the ECS, the NSCS shelf as well as the TWS in winter 2008.

BGD
10, 3891–3923, 2013

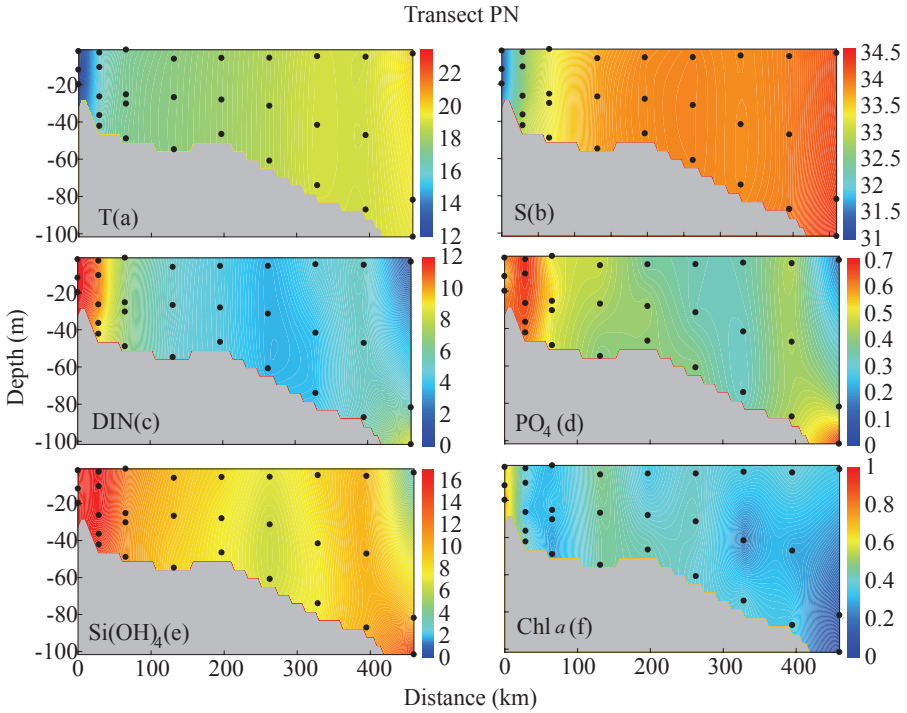

Fig. 3. Transectional distributions of T (**a**, °C), S **(b)**, DIN (**c**, μmol L^{-1}), PO_4 (**d**, μmol L^{-1}), $Si(OH)_4$ (**e**, μmol L^{-1}), and Chl *a* (**f**, mg m^{-3}) in Transect PN on the ECS in winter 2008.

BGD
10, 3891–3923, 2013

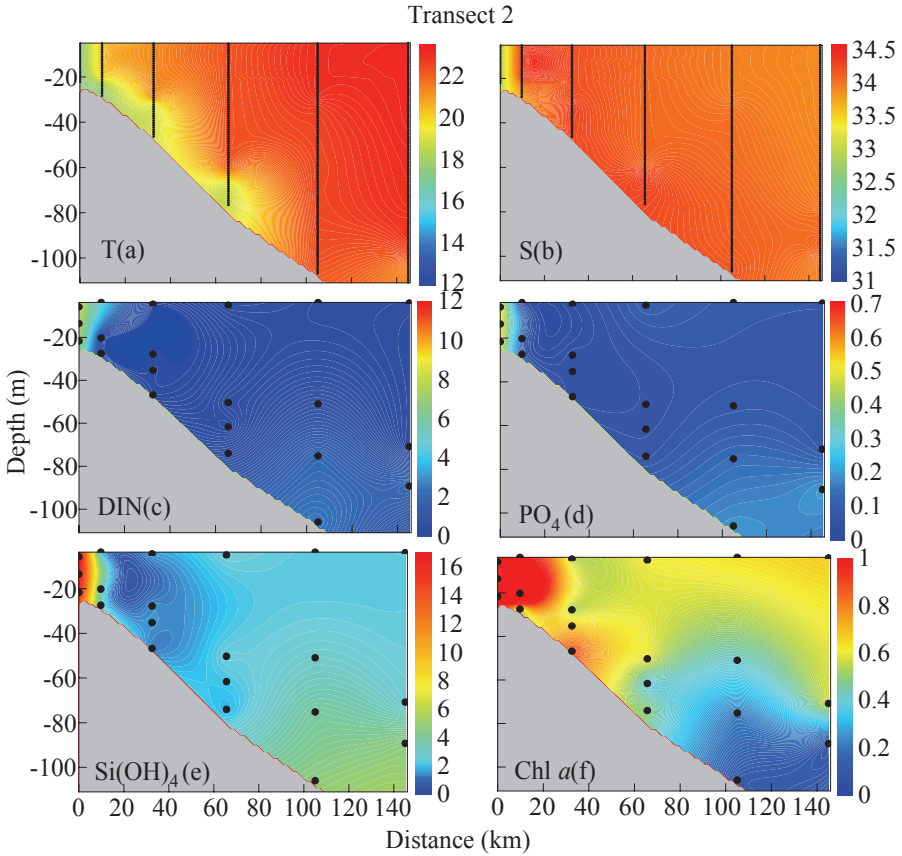

Fig. 4. Transectional distributions of T (**a**, °C), S **b**, DIN (**c**, μmol L^{-1}), PO_4 (**d**, μmol L^{-1}), $Si(OH)_4$ (**e**, μmol L^{-1}), and Chl *a* (**f**, mg m^{-3}) in Transect 2 on the NSCS shelf in winter 2008.

BGD
10, 3891–3923, 2013

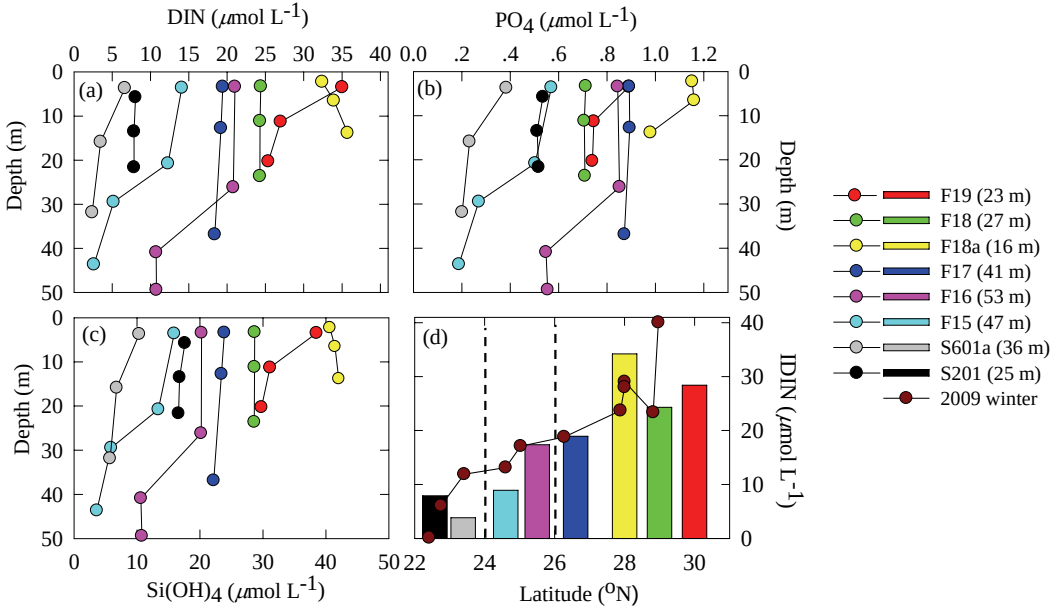

Fig. 5. Vertical profiles of nutrients (**a**: DIN, **b**: PO_4 and **c**: $Si(OH)_4$) in the CCC stream from the ECS to the NSCS shelf via the TWS in winter 2008. Stations F19–F17 are for the ECS segment, F16–F15 for the TWS segment and S601a-S201 for the NESCS segment. Averaged depth-integrated DIN (IDIN, μmol L^{-1}) in winter 2008 (color bars) and winter 2009 (dots) **(d)**. Water depth for each station in winter 2008 was also shown.

BGD
10, 3891–3923, 2013

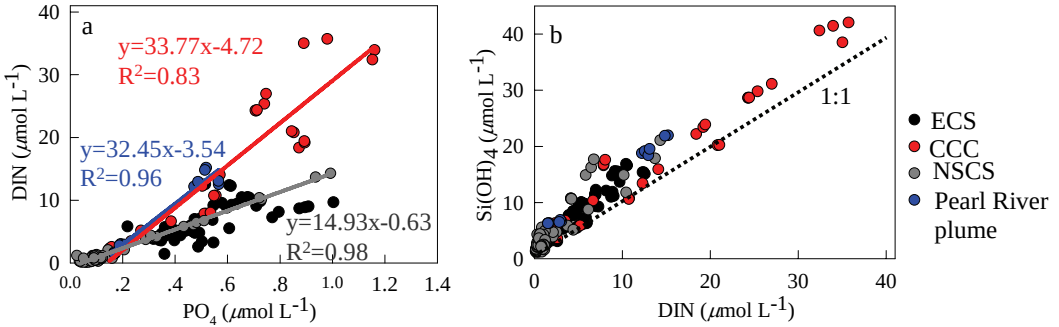

Fig. 6. Correlations between DIN and PO_4 **(a)**, $Si(OH)_4$ and DIN **(b)** in the different water masses on the ECS and the NSCS shelf through the TWS in winter 2008. Red and grey lines indicate the regression line of DIN and PO_4 in the CCC and the NSCS shelf.

BGD
10, 3891–3923, 2013

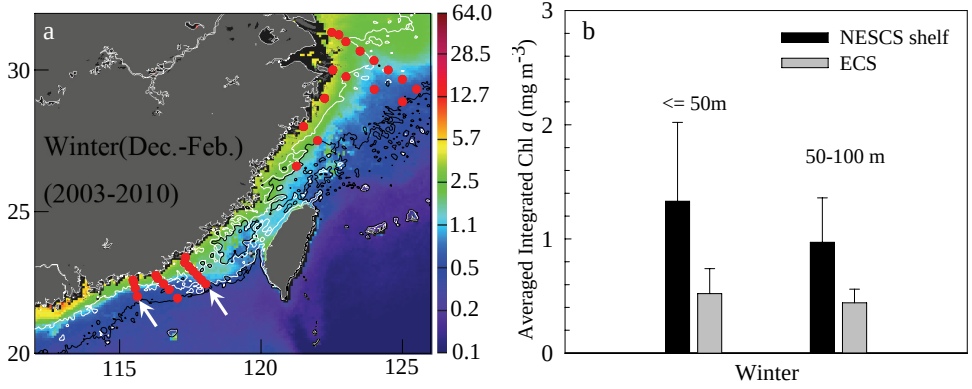

Fig. 7. (a) Averaged Moderate Resolution Imaging Spectroradiometer (MODIS) Chl *a* (mg m^{-3}) with 9 km spatial resolutions over the ECS-TWS-NSCS shelf in winter (December–February) from 2003 to 2010 (http://oceancolor.gsfc.nasa.gov/ftp.html). White and black indicated the isobaths of 50 m and 100 m. White arrows in **(a)** indicated the NESCS shelf where isobaths up to 100 m. **(b)** Averaged depth integrated Chl *a* (mg m^{-3}) on the ECS and the NESCS shelf ($\leq$ 100 m isobath) in winter 2008 (stations were marked by red dots in **a**). Error bars represented the spatial variations.

BGD
10, 3891–3923, 2013

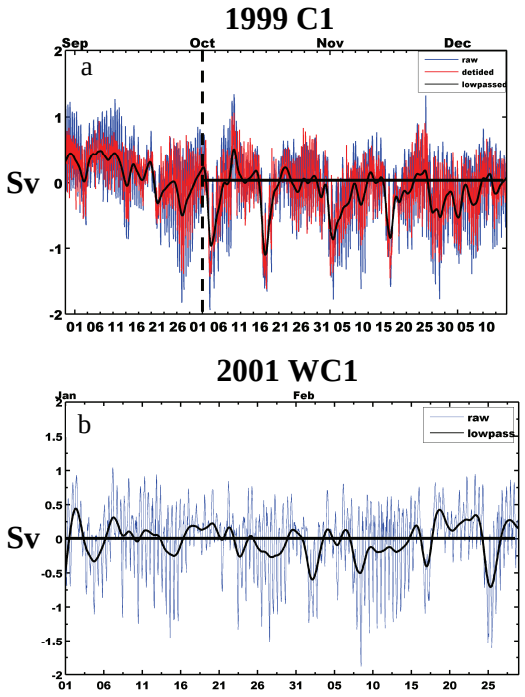

Fig. 8. Two sets of time series along-strait current volume transport (T_T, in units of Sv, $1\,\mathrm{Sv} = 10^6\,\mathrm{m^3\,s^{-1}}$) at C1 (24.96° N, 119.47° E) and WC1 (24.80° N, 119.49° E) during 1 September–14 December 1999 **(a)** and 1 January–28 February 2001 **(b)**, respectively. The current velocities were measured by bottom-mounted Acoustic Doppler Current Profile (bm-ADCP) which was deployed within 50 m isobath (~ 44 m) in the western TWS. T_T was calculated with raw and 30 h low pass filtered velocity data, assuming the coastal width of 30 km (to ~ 119.2° E). Negative values represented the southward velocities. T_T in winter 1999 we adopted was from 1 October–14 December, when northeast monsoon was prevailing. Detailed information was described in Jan et al. (2006).

BGD
10, 3891–3923, 2013

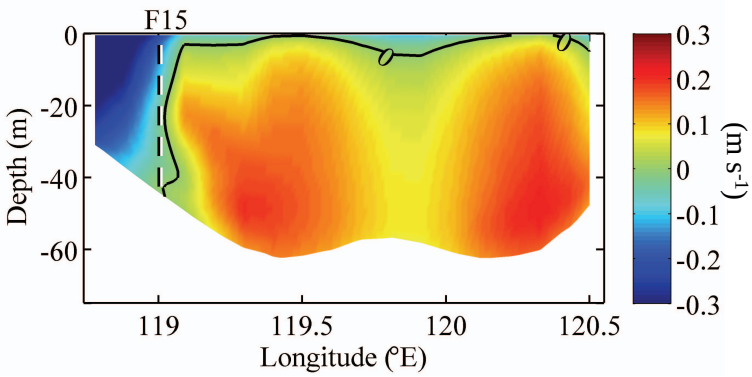

Fig. 9. The model-derived structure of current velocity ($m\,s^{-1}$) along 24.6° N in TWS in winter (December, January and February). The negative/positive values indicated the southward/northward velocities. Southward T_T was integrated between 118.84° E and 119.0° E (i.e., coastal width was ~17.5 km), and water depth 44 m, indicated by the dashed line. The zero contours appeared in heavy line.

BGD
10, 3891–3923, 2013